An idealized semi-empirical framework for modeling the Madden-Julian oscillation

Adam H. Sobel [1]

Department of Applied Physics and Applied Mathematics

Department of Earth and Environmental Sciences

Lamont-Doherty Earth Observatory

Columbia University, New York, NY,

and

Eric D. Maloney

Department of Atmospheric Sciences, Colorado State University, Fort Collins, CO.,

[1] *Corresponding Author Address:* Adam Sobel, Columbia University, Dept. of Applied Physics and Applied Mathematics, 500 W. 120th St., Rm. 217, New York, NY 10027 USA. E-mail: ahs129@columbia.edu

ABSTRACT

We present a simple semi-empirical model for MJO studies in which it is assumed that the MJO is a moisture mode destabilized by surface flux and cloud-radiative feedbacks. The model is one-dimensional in longitude; vertical and meridional structure are entirely implicit. The only prognostic variable is column water vapor, W. The zonal wind field is an instantaneous, diagnostic function of the precipitation field.

The linearized version of the model has only westward-propagating (relative to the mean flow) unstable modes, because wind-induced surface latent heat flux anomalies occur to the west of precipitation anomalies. The maximum growth rate occurs at a synoptic- to planetary-scale wavelength at which the correlation between precipitation and surface latent heat flux is maximized; this wavelength is proportional to the horizontal scale associated with the assumed diagnostic wind response to precipitation anomalies.

The nonlinear version of the model has behavior that can be qualitatively different from the linear modes, and is strongly influenced by horizontal advection of moisture. The nonlinear solutions are very sensitive to small shifts in the phasing of wind and precipitation. Under some circumstances nonlinear eastward-propagating disturbances emerge on a state of mean background westerlies. These disturbances have a shock-like discontinuous jump in humidity and rainfall at the leading edge; humidity decreases linearly and precipitation decreases exponentially to the west. Use of a wind structure consistent with off-equatorial heating makes this nonlinear mode more likely to emerge.

1. Introduction

We propose a highly idealized model for theoretical studies of the Madden-Julian oscillation (MJO; Madden and Julian 1971). In its current form, we do not consider the model to constitute a fully successful theory for the MJO. It is, rather, a straightforward extension of certain even simpler models, in a direction of increasing fidelity to the realities of the MJO. The model makes a number of strong simplifying assumptions, motivated by observations, theory, and particularly recent numerical modeling (e.g., Maloney et al. 2010), which embody a set of hypotheses about the dynamics of the MJO:

1. The MJO is a "moisture mode", meaning that it depends essentially on a prognostic humidity equation and is not analogous to any dynamical mode which occurs in a dry atmosphere. Moisture modes (sometimes called by other names) have been studied previously in many other models with varying degrees of complexity (Neelin and Yu 1994; Sobel et al. 2001; Fuchs and Raymond 2002, 2005, 2007; Sobel and Bretherton 2003; Raymond and Fuchs 2009; Sugiyama 2009a,b; Majda and Stechmann 2009; Maloney et al. 2010; Kuang 2011; Andersen and Kuang 2011). Growth of such disturbances is governed by feedbacks that increase moisture anomalies, and their propagation is governed by processes that make moisture anomalies move horizontally. Horizontal moisture advection in particular may be important (e.g., Maloney et al. 2010). According to this hypothesis, the MJO is not a Kelvin wave; Kelvin waves may play a role in its dynamics, but the MJO does not propagate by interactions between buoyancy and pressure gradients as a Kelvin wave does. It may be that the phenomenon known as the MJO consists of two dynamically different disturbances, one in the Indian

and western Pacific basins which is distinct from convectively coupled Kelvin waves (Wheeler and Kiladis 1999; Kiladis et al. 2009), and one in the central and eastern Pacific and Atlantic basins which is essentially Kelvin wave-like. We are interested in the former.

2. Thermodynamic feedbacks are important energy sources for the MJO. We refer specifically to feedbacks between MJO disturbances and the sources and sinks of column-integrated moist static energy, namely surface turbulent fluxes (Emanuel 1987; Neelin et al. 1987) and radiative cooling throughout the column (Raymond 2000; Fuchs and Raymond 2002). Evidence that these feedbacks are important to the MJO comes from both observations and numerical model studies, and is reviewed by Sobel et al. (2008, 2010). Negative gross moist stability (Raymond and Fuchs 2009; Raymond et al. 2009). This is not explored directly here, but could be by a straightforward extension of the model.

3. Both vertical and meridional structure can be taken implicit. Our model has only a single prognostic PDE in longitude and time. The prognostic variable is total column water vapor. We assume that the meridional and vertical structures are known but that the processes that determine them can be taken for granted. This could be argued more formally by projection on a set of basis functions, in the meridional (Majda and Khouider 2001) or vertical (e.g., Neelin and Zeng 2000). While our single prognostic variable would be formally consistent with a single basis function in the vertical, some key effects of variable structure can nonetheless be captured implicitly by extensions of the model presented here that do not require changing its basic form. For example, the

effect of variable vertical structure on gross moist stability (e.g., Haertel et al. 2008) might be represented by a parameterization of the gross moist stability as a function of humidity or zonal wind.

4. Convection in the MJO is in a state of quasi-equilibrium with its forcings. We assume that the precipitation and convective heating can at any moment be taken to be an instantaneous function of the thermodynamic state.

5. Large-scale wind anomalies associated with the MJO can be taken to be a quasi-steady response to heating. That is, the wind field can be diagnosed instantaneously from the heating field at a given moment. This amounts to an assumption that the time scale for the steady response to a fixed heat source to be established is short compared to the MJO frequency. This assumption allows a strong simplification of the model. It is suggested by observational studies showing a broadly Gill (1980) - type structure to MJO wind anomalies (e.g., Chen et al. 1996), and is shown explicitly to be the case in an idealized numerical model by Sugiyama (2009b). A plausible structure of the wind response to heating is specified in this work based on the Gill model, but we view the more precise definition of this structure as a target for future study. Processes not explicitly included, such as convective momentum transport (e.g., Houze et al. 2000; Tung and Yanai 200a,b; Lin et al. 2004; Miyakawa et al. 2011), could be included implicitly by their influence on the projection operator which relates wind to heating. The model behavior is extremely sensitive to the details of this assumed wind structure.

6. Ocean coupling is not essential. A large number of GCM studies indicate that while ocean coupling may improve the simulation of the MJO, it is not essential to the

existence of the MJO (Waliser et al. 1999; Hendon 2000; Kemball-Cook et al. 2002; Inness and Slingo 2003; Zheng et al. 2004; Maloney and Sobel 2004; Grabowski 2006; Fu et al. 2007). The essential mechanisms of MJO development, maintenance, propagation and scale selection should operate in an uncoupled context.

In section 2 we introduce the model. In section 3 we linearize the model and show the properties of its linear normal modes. In section 4 we present a few representative numerical solutions of the fully nonlinear model, and in section 5 we conclude.

2. Model framework

a. Basic equations

The only prognostic equation for the atmosphere in our model is one for column-integrated water vapor, $W(x,t)$:

$$\frac{dW}{dt} - M_q\Delta = E - P + k_W\frac{\partial^2 W}{\partial x^2}, \tag{1}$$

where d/dt is a material derivative following the zonal flow (discussed further below); E is surface evaporation and P precipitation; and M_q is a gross moisture stratification (Neelin 1997) which is the proportionality coefficient relating the column-integrated moisture convergence to the upper-level mass divergence, Δ, associated with the baroclinic flow. The last term is zonal diffusion with diffusivity k_W. The dry static energy equation is made diagnostic by the weak temperature gradient (WTG) approximation:

$$M_s\Delta = P - R. \tag{2}$$

where M_s is the gross dry stability and R is vertically integrated radiative cooling. We have neglected the surface sensible heat flux — a good approximation over tropical oceans — and consistent with the assumption that horizontal temperature gradients are small, neglected horizontal diffusion of dry static energy. The WTG approximation need not rule out all effects of temperature variations; those which are correlated with moisture variations can be included implicitly. The dynamics of gravity and Kelvin wave propagation, on the other hand, are excluded. Adding (1) and (2) gives the moist static energy equation:

$$\frac{dW}{dt} = -\Delta M + E - R + k_W \frac{\partial^2 W}{\partial x^2}, \tag{3}$$

where $M = M_s - M_q$ is the gross moist stability (Neelin and Held 1987; Neelin 1997). Eliminating the divergence using (2) in (3), and expanding the total derivative on the LHS gives

$$\frac{dW}{dt} = \frac{\partial W}{\partial t} + u\frac{\partial W}{\partial x} = -\tilde{M}P + E - (1-\tilde{M})R + k\frac{\partial^2 W}{\partial x^2}, \tag{4}$$

where $u(x,t)$ is an advecting zonal wind at a nominal steering level, and $\tilde{M} = M/M_s$ is the "normalized gross moist stability" (defined slightly differently than in Raymond (2009), in that those authors normalize by moisture convergence rather than dry static energy divergence).

b. Time and zonal mean budgets

Our model domain represents a longitudinal section through a domain with implicit latitudinal structure. We do not assume, however, that the flow lies fully in the zonal plane with zero meridional component, and accordingly **we do not require that** $\Delta = -\partial u/\partial x$**.** Thus the mass, energy, and moisture budgets do not close in the domain integral. They are

in weak temperature gradient balance with an implicit Hadley circulation. In the special case in which time dependence, horizontal advection and diffusion are all negligible, the precipitation at any x is given by the single-column local expression

$$P = \tilde{M}^{-1}[E - (1 - \tilde{M})R]. \tag{5}$$

While advection in particular is generally not negligible, (5) is nonetheless useful in understanding some basic properties of the model, as discussed further below. In the general case, integrating (4) over the domain in x gives

$$\frac{\partial}{\partial t}\int W dx = \int [-\tilde{M}P + E - (1 - \tilde{M})R - u\frac{\partial W}{\partial x} + k_W \frac{\partial^2 W}{\partial x^2}]dx. \tag{6}$$

In steady state, the precipitation satisfies

$$\int \tilde{M}P dx = \int [E - (1 - \tilde{M})R - u\frac{\partial W}{\partial x} + k_W \frac{\partial^2 W}{\partial x^2}]dx. \tag{7}$$

This equation does not give a closed relationship between domain-averaged quantities; for example, even if E and R are specified and $\tilde{M}$ is taken constant, computation of the advection term requires knowledge of the longitudinal structure of u and W. Because Δ and u are not uniquely related, the explicit horizontal advective transport can have a nonzero domain average and it is not helpful to phrase the model in flux form. Equation (7) simply shows the nature of the local zonal mean WTG balance. While there are implicit latitudinal transports, at this stage we do not explicitly model latitudinal transports associated with meridional gradients — there are no advective or diffusive terms involving derivatives of W with respect to latitude. Such terms may under some circumstances be quantitatively non-negligible, and could be added in parameterized form.

Taking the zonal wind u to advect the entire column water vapor, as in (4), may overestimate the effect of horizonal advection. Horizontal advection of moisture is indeed likely to be greatest in the lower free troposphere, as illustrated by budget analyses from simulations (e.g., Maloney 2009; Maloney et al. 2010), but the zonal wind tends to change sign with height in MJO events while the moisture gradient generally does not. In the quasi-equilibrium tropical circulation model (QTCM), for example (Neelin and Zeng 2000; Zeng et al. 2000), the horizontal advection term computed from explicit projection on the assumed vertical structures is multiplied by a coefficient on the order of 0.3 to capture this. On the other hand, the lower tropospheric water vapor is presumably the more important for controlling convection while the upper tropospheric water vapor is expected to vary more as a passive response to convection (e.g., Sherwood 1999; Sobel et al. 2004), so one could argue that for the model to capture that feedback it should weight lower-level advection more heavily.

c. Model physics

Our convective closure models P as a function of W, $P = P(W)$. The relationship between precipitation and column water vapor is the subject of both theoretical and observational work (Raymond 2000; Bretherton et al. 2004; Peters and Neelin 2006; Neelin et al. 2009), and it has been suggested that the simulation of the MJO in global models is sensitive to it (Benedict and Randall 2009; Zhu et al. 2009). Here, we choose $P(W)$ according to the observational study of Bretherton et al. (2004):

$$P = \exp[a_d(F - r_d)], \tag{8}$$

with $a_d = 15.6$, $r_d = 0.603$, and F the saturation fraction

$$F = \frac{W}{W_{max}}, \tag{9}$$

with W_{max} the saturation column water vapor. Here W_{max} is chosen to be 70 mm, consistent with typical warm pool values.

We parameterize atmospheric radiative cooling by a clear-sky term, taken constant, plus a cloud-radiative feedback term taken proportional to precipitation, with the additional requirement that the net effect of radiation must be to cool, not heat the atmosphere:

$$R = \max(R_0 - rP, 0). \tag{10}$$

Our control value of r is 0.1, broadly consistent with that estimated from observations (Bretherton and Sobel 2002; Lin and Mapes 2004). We expect that this radiative feedback will be destabilizing and assist in the development and maintenance of intraseasonal disturbances (e.g., Raymond 2001, Sobel and Gildor 2003, Bony and Emanuel 2005; Zurovac-Jevtic et al. 2006; Sobel et al. 2008, 2010, Andersen and Kuang 2011, Landu and Maloney 2011).

Surface evaporation is parameterized as a function of steering level wind speed:

$$E = E_0 + E' = E_0 + C_u|u|. \tag{11}$$

The dependence on wind speed is motivated by results from the simulation of Maloney et al. (2010). Fig. 1 shows daily mean values of surface latent heat flux and 850 hPa zonal wind from the simulation described in that study; values shown in fig. 1 are taken only from the warm pool region where the simulated MJO disturbances are most active. While the latent heat flux in these simulations does depend on an air-sea humidity difference according to a standard bulk formula, to first order the wind speed at 850 hPa appears to contain

sufficient information to compute the flux. Parameterizing E as a function of $|u|$ but not W allows us to avoid representing the surface air humidity as a function of column water vapor, something that is difficult to do well without an explicit boundary layer.

The normalized gross moist stability, $\tilde{M}$, is taken constant and positive in this study. Variable $\tilde{M}$ can be included, and most obviously could be parameterized as a function of W (such dependence would be required to write a closed moisture budget in flux form in the zonal plane, but as discussed above our system is open with implicit meridional transport).

With the radiative parameterization (10), if P remains smaller than $R_0 r^{-1}$, the precipitation in steady state for the special case of negligible horizontal advection and diffusion, (5), can be written

$$\tilde{M}_{eff} P = E - (1 - \tilde{M}) R_0, \tag{12}$$

where $\tilde{M}_{eff} = \tilde{M}(1 + r) - r$ is a normalized "effective gross moist stability" including radiative feedbacks (e.g., Bretherton and Sobel 2002; Su and Neelin 2002). For our control parameters, $M_{eff} = 0.01$, while E and $(1-\tilde{M})R_0$ are typically close in value. Thus the steady state precipitation in this idealized case results from a delicate balance in the moist static energy budget in which the forcing and effective gross moist stability are both quite small. Our actual solutions (in the nonlinear regime) are both unsteady and strongly influenced by horizontal advection but nonetheless obey a similar constraint to (7). As the zonal mean surface evaporation E is strongly controlled by the wind and thus the amplitude of propagating disturbances, the disturbances and mean state are in general strongly coupled. Tuning is required to keep the mean precipitation reasonably close to values observed in earth's tropics. While this is not in principle a desirable feature, it appears to be broadly

consistent with observations which show a gross moist stability not clearly distinguishable from zero in the rainiest parts of the tropics (Back and Bretherton 2006).

d. Zonal wind as a diagnostic function of precipitation

We impose a constant background wind, U, such that $u(x,t) = U + u'(x,t)$. We do this even in the nonlinear model. The constant background wind reflects the influence of implied Hadley and Walker circulations unresolved by our model. The perturbation $u'(x,t)$ need not have zero mean. If δ were proportional to $\partial u/\partial x$, as in idealized "mock Walker" models (e.g., Bretherton and Sobel 2002) we could simply integrate δ to find u'. Instead we assume that u' is both divergent and rotational, but that it can be computed instantaneously from the precipitation via a projection operator, similar to a Green's function:

$$u'(x,t) = \int G(x|x')P(x',t)dx'. \tag{13}$$

We can determine G empirically or theoretically. Here, we derive G from the solutions of Gill (1980) to the linear shallow water system on an equatorial beta plane subject to a localized mass source forcing and Rayleigh damping on the mass and momentum fields, but also allow an ad hoc zonal shift of the wind response relative to the heating.

$$G(x|x') = -Ae^{-[x-(x'+\delta)]/L}, \quad x > x + \delta', \tag{14}$$

$$G(x|x') = 3Ae^{3[x-(x'+\delta)]/L}, \quad x < x' + \delta. \tag{15}$$

with A and L constants. For $\delta = 0$, this can be derived from Gill's model in the equatorially symmetric case if the heating has the meridional structure assumed by Gill, but is a delta function in longitude. The length scale L can be interpreted as the group velocity of free

Kelvin waves (for $x > x'$) or Rossby waves (for $x < x'$) divided by the Rayleigh damping rate (e.g., Sarachik and Cane 2010, pp. 157-162). The factor of 3 expresses the fact that the group velocity of Kelvin waves is three times that of long Rossby waves. Use of a Gill solution for an off-equatorial forcing (discussed below) strengthens the westerly component relative to the easterly (if the near-equatorial wind is still taken to be the relevant one) but does not significantly shift the relative longitudinal position of the peak westerlies; sensitivity of the model behavior to this change is discussed in section 4c.

In this study we choose the length scale L to be 1500 km. This is consistent with an equivalent depth of 40m (Kelvin wave speed 20 m s^{-1}) if the dissipation time scale for the wave response to heating is 1d, characteristic of boundary layer drag (arguably appropriate for surface wind, though too small for free-tropospheric wind). The value 40m is slightly higher than that found by Wheeler and Kiladis (1999) for convectively coupled waves, but considerably smaller than would be appropriate for dry equatorial waves. While there is a temperature and wind response that propagates at around 40 $m\ s^{-1}$ (Bantzer and Wallace 1996), the convective signal does not propagate this quickly. Our value of 20 $m\ s^{-1}$ is consistent with the speed found in observations by Maloney and Shaman (2008) for the observed propagation of the MJO into the Atlantic, and that found in GCM simulations for the Kelvin wave response to the switch-on of a localized SST anomaly (Maloney and Sobel 2007). Sensitivity of our model to L is clear in the linear calculations, below; sensitivity to it in the nonlinear system is deferred to future work.

The parameter δ is a distance by which the response G is shifted relative to where it would be relative to that obtained from (14)-(15). We adopt this device to allow the transition between easterly and westerly events to depart slightly from what one would expect from the

Gill solution. Such departures could result from a number of factors not present in the highly idealized linear shallow water system including more complex vertical structure, convective momentum transport (Houze et al. 2000; Tung and Yanai 2002a,b; Lin et al. 2004; Miyakawa et al. 2011), meridional momentum transport by synoptic-scale disturbances (Biello et al. 2007; Showman and Polvani 2010), or nonlinearity in the direct flow response to MJO-scale heating (Gill and Phlips 1986). These factors might well change the structure of G as well as its phase; such structural changes may be of interest in future studies but are not considered here. We require δ to be relatively small compared to L; the largest value used in this study is $4L/15$, or $0.27L$. The amplitude A is chosen so that precipitation anomalies of planetary spatial scale have wind anomalies whose magnitude in $m\ s^{-1}$ is comparable to that of the precipitation anomalies in $mm\ d^{-1}$, as occurs in the simulations of Maloney et al. (2010).

e. Summary remarks on model construction

In essence, the present model can be viewed as an extension of a simple WTG single-column model (e.g., Sobel and Gildor 2003; see also Maloney and Sobel 2004) to incorporate one horizontal dimension (longitude). As in such models, the present model's essential dynamics include those relating moisture and convection under the weak temperature gradient approximation and a quasi-equilibrium convective closure, and cloud-radiative feedbacks. These processes have been found to cause spontaneous self-aggregation of convection in large-domain cloud resolving simulations (Bretherton et al. 2005), behavior which is captured by the existence of multiple equilibria (convecting and non-convecting) in WTG single-column (Sobel et al. 2007) or small-domain cloud-resolving models (Sessions et al. 2010). The key

new additions here result from the addition of horizontal structure, with horizontal wind modeled as a quasi-steady response to precipitation. This allows horizontal advection and large-scale wind-evaporation (WISHE) feedbacks to be explicitly included.

The lack of explicit, self-consistent representation of meridional and vertical structure (basis functions, vertical layers, etc.) results from a conscious choice. We hypothesize that a model of the form above with suitable physics may focus our attention usefully on understanding the roles of the different processes as captured by key bulk parameters — e.g., the gross moist stability $\tilde{M}$, response of wind to heating via L and δ, etc. — and the magnitudes of the terms necessary to generate MJO-like disturbances at some desired level of realism. We postpone any attempt at determining how the full three-dimensional structure of the primitive equations should best be truncated to achieve a self-consistent representation of those processes in terms of explicit but simple vertical and horizontal structures. It is in this sense that we refer to the model as "semi-empirical".

3. Linear analysis

We linearize the model about a background state W_0,

$$W = W_0 + W'(x,t). \tag{16}$$

The background state is also assumed to have a uniform zonal wind U, so that the total wind is $U + u'(x,t)$. The linearized model is

$$\frac{\partial W'}{\partial t} + U\frac{\partial W'}{\partial x} = -\tilde{M}P' + E' - (1-\tilde{M})R' + k_w\frac{\partial^2 W'}{\partial x^2,} \tag{17}$$

We linearize our convective parameterization about the state $W = W_0$, $P = P_0 = \exp[a_d((W_0/W_{max}) - r_d)]$, thus obtaining

$$P' = \frac{W'}{\tau_c}, \tag{18}$$

where

$$\tau_c = \frac{W_{max}}{a_d P_0} = a_d^{-1} W_{max} \exp[-a_d((W_0/W_{max}) - r_d)]. \tag{19}$$

Our linearized radiative perturbations are then

$$R' = -r\tau_c^{-1} W', \tag{20}$$

while, if we assume westerly mean winds, our latent heat flux is

$$E' = C_u u'. \tag{21}$$

Now assuming sinusoidal perturbations $W' = \mathcal{W} e^{i(kx-ct)}$, with $\mathcal{W}$ a complex amplitude and c a (potentially) complex phase speed, and substituting we obtain

$$ik(U-c)W' = -\tau_c^{-1}[\tilde{M}_{eff} + k_w k^2]W' + C_u u'. \tag{22}$$

With a projection function of the form (14)-(15) and the linearized convective parameterization (18), u' can be found analytically from (13),

$$u' = \Gamma(k) P' = \Gamma(k) \frac{W'}{\tau_c}, \tag{23}$$

where

$$\Gamma(k) = \frac{4Ae^{-ik\delta}[\frac{2k^2}{L} + i(\frac{3k}{L^2} + k^3)]}{(9/L^2 + k^2)(1/L^2 + k^2)}. \tag{24}$$

From this it follows that the phase angle by which u' lags P' is

$$\alpha = \tan^{-1}(\frac{3}{2kL} + \frac{kL}{2}) - k\delta. \tag{25}$$

For $\delta = 0$, the zonal wind and precipitation fields are thus in quadrature when the dimensionless ratio of length scales kL is either zero (long wavelength $2\pi/k$ compared to wind decay scale L) or infinite (short wavelength). For $\delta = 0$ the wind is most nearly in phase with precipitation at the optimal value $kL = \sqrt{3}$ at which $\alpha = \tan^{-1}\sqrt{3} = \pi/3$; for δ small (compared to $\pi/3k$) but nonzero, the minimum phase lag is $\alpha = \pi/3 - k\delta$.

The importance of the phase lag between wind and precipitation is apparent if we take the linear atmospheric equation (17), multiply by W', substitute $P' = \tau_c^{-1} W'$ and $R' = -rP'$, and integrate over the domain, assumed periodic, to obtain an equation for the variance of W':

$$\frac{\partial}{\partial t}\int \frac{1}{2} W'^2 dx = -\tau_c^{-1}\tilde{M}_{eff}\int W'^2 dx + \int E'W' dx - k_w \int (\frac{\partial W'}{\partial x})^2 dx. \tag{26}$$

While (26) assumes a periodic domain, it does not assume sinusoidal perturbations. The last term on the RHS is negative definite, and the first is as well if M_{eff} is positive. In that case amplitude growth can result only from the second term, which is the covariance of surface latent heat flux and column water vapor. Under our assumptions this wind-evaporation feedback term will be positive in general for a westerly mean state, and perturbations whose maximum winds are westerly and lag the precipitation with respect to longitude. This is fundamentally different from a convectively coupled Kelvin wave destabilized by wind-evaporation feedback in an easterly flow (Emanuel 1987; Neelin et al. 1987).

For the linear system, using (23), (22) becomes

$$ik(U-c)W' = \tau_c^{-1}[r - \tilde{M}(1+r) + C_u\Gamma - k_w k^2]W', \tag{27}$$

or

$$c = U + \frac{\tilde{M}_{eff} - C_u\Gamma + k_w k^2}{ik\tau_c}, \tag{28}$$

The phase speed c and wind-precipitation proportionality factor Γ are both complex in general; all other coefficients in (27) are real. The disturbances propagate at a real phase speed $Re(c)$, while $Im(c)k$ is the linear growth rate. These two quantities are shown in fig. 2 for the parameters shown in table 1, except that k_w is set to zero; the value used in the nonlinear calculations is sufficiently small that including it does not significantly change the results (not shown). In these calculations the mean state column water vapor is $W_0 = 45mm$, resulting in a convective time scale $\tau_c = 2.4$ d. The growth rate and phase speed are both inversely proportional to τ_c, as can be seen from (28). The growth rate has its maximum at zonal wave number 7.3, or a wavelength of 5440 km, consistent with the value $kL = \sqrt{3}$ as discussed above. A larger value of the parameter L would of course lead to a larger wavelength at the maximum growth rate.

Fig. 3 shows the same calculations for a range of values in the key parameters r and δ. We see that increasing either parameter increases the growth rate, while the shapes of the curves remain qualitatively similar as these two parameters are varied

Fig. 4 shows the sensitivity to the inverse convective time scale, τ_c^{-1}, which grows exponentially with the background moisture W_0 according to (19). The growth rate increases rapidly with τ_c^{-1}, as does the (westward) phase speed. Logarithmic scales are used on the y-axis of both plots. For large τ_c^{-1} (small τ_c; the smallest value shown is 0.03 d) the growth rates are so large that nonlinearity would rapidly become important, and the phase speed is also so large as to render multiple assumptions of the model (e.g., quasi-stationarity of wind response to heating) invalid.

4. Nonlinear numerical solutions

a. Numerical model configuration and parameters

We solve the nonlinear system numerically on a periodic domain of length 40,000 km, with 1000 grid points so the horizontal grid spacing is 40 km. We use a first-order upwind scheme for horizontal advection and a leapfrog time stepping procedure with a Robert-Asselin filter and a time step of 0.001 days. Simulations are initialized somewhat arbitrarily with the initial condition

$$W = W_0 + \Delta W \sin(\frac{\pi x}{L_m}),$$

where here $W_0 = 50$mm, $\Delta W = 2$mm, and $L_m = 40000$km is the domain size. It is found through experimentation that the qualitative results of interest are not sensitive to the initial conditions, though our exploration of the initial conditions is not at all exhaustive.

We impose a background westerly wind of 5 $m\ s^{-1}$. This influences both horizontal advection and surface fluxes. We imagine that our domain, despite having an extent approximately equal to the circumference of the earth, consists solely of a "warm pool", or region of relatively high sea surface temperature, while elsewhere (at both other latitudes and longitudes, though neither are explicitly included) the SST is lower. Thus precipitation is focused on the warm pool, and the quasi-steady response includes low-level westerly winds, as is the case in the tropical Indian and western Pacific oceans on earth.

b. Results

Fig. 5 shows Hovmoeller plots of saturation fraction from calculations with parameters shown in table 1 and δ = +400, 0, and -400 km. The first two show a combination of eastward and westward propagation for the first 20-30 days followed by predominantly eastward propagation thereafter, while the third shows westward propagation. In the $\delta = 400$ km solution in the left panel, the eastward propagation speed is approximately that of the background wind, 5 $m\ s^{-1}$. The dominant spatial structures have wave number two for $\delta = 400$ km, and wave numbers 4-8 in the latter two calculations (as made more apparent in the figures below). We have integrated the model for 800 days in each case, and the behavior after the time shown in the figures is quite regular. In particular for δ = +400, the brief interval of westward propagation around day 100 does not recur; rather constant eastward propagation persists and the structures shown in fig. 6 (below) are unchanged at day 800 compared to those shown in that figure.

Figs. 6-8 show snapshots of precipitation and perturbation zonal wind (left panels) and water vapor path and surface evaporation (right panels) on day 128 for the same three calculations shown in fig. 5, in the same order. In fig. 6 we see two isolated peaks in precipitation, with roughly exponential increases on the western sides and then step-like decreases back down to a zero background on the eastern sides. This structure (including the number of peaks, two) appears at least qualitatively independent of initial conditions, for a range of initial perturbations we have tried (not shown). The zonal wind has westerlies roughly in phase with precipitation with strong easterlies ahead in the dry regions. The water vapor path in this solution has a nearly triangular wave pattern, with a linear increase

followed by a step decrease. The latent heat flux has two peaks separated by a sharp minimum at the point where the wind perturbation switches from easterly to westerly.

Fig. 7 shows the same fields as in fig. 6 but for $\delta = 0$. Recall from fig. 5 that there is still some eastward propagation in this solution (also recall that there is a background eastward wind of 5 $m\ s^{-1}$) but the perturbations are smaller in amplitude and less organized on the planetary scale than in Fig. 6. Some of the precipitation features resemble the sharp structures in fig. 6, but overall the precipitation field and water vapor fields are both smoother in this case. Close inspection reveals that E lags W by more than in the previous figure, as expected. These differences are still more pronounced in fig. 8, with $\delta = -400$ km. Recall from 5 that the disturbances in this solution move rapidly westward. The structures in all fields are smoother and closer to sinusoidal than those in figs. 6 and 7. The precipitation variations, from maximum to minimum, are roughly a factor of three smaller than those in fig. 6, while the variations in W are smaller by a factor of five. The lack of proportionality is due to the fact that the solution with $\delta = -400$ km is considerably moister in the mean, resulting in a stronger response to small W variations (smaller τ_c, in the linearized model).

The interesting feature in these solutions is the emergence of the highly nonlinear solution for positive δ. While simply shifting G as we have done is *ad hoc*, the results demonstrate the strong sensitivity of this system to the phase relationship between zonal wind and precipitation. The existence of these nonlinear solutions depends on both horizontal advection by the perturbation winds (an inherently nonlinear effect) as well as the mean flow and on the shifting of E forward so that it is more nearly in phase with W and P (an effect which is present in the linearized model as well). When either of these effects are disabled, the nonlinear mode shown in fig. 6 is strongly weakened or otherwise altered (not shown). An

exploration of other parameter choices (not shown) suggests that self-advection is the more important of the two effects in generating this mode. The step discontinuity in W at the eastern side of the rainy region is reminiscent of the precipitation fronts which can occur in a quasi-linear system without nonlinear horizontal advection (Frierson et al. 2004; Stechmann and Majda 2006; Pauluis et al. 2008). Here, however, it is clearly a result of nonlinear advection, as it corresponds with strong zonal confluence. The effect of this confluence can be seen in the initial $\sim 20-30$d of the left panel in fig. 5, where eastward- and westward-moving moist regions on either side of $x = 0$ move towards each other before colliding near $x = 0$ around $50d$ and coalescing into the narrower structure evident in fig. 6.

While the eastward propagation and planetary horizontal scale of the nonlinear mode are encouraging, the discontinuity at the leading edge is not MJO-like. Observations show that the transition from suppressed to active phase is as gradual as that from active back to suppressed, if not more so (Kemball-Cook and Weare 2001; Kiladis et al. 2005; Benedict and Randall 2007). Better representation of the processes that lead to the slow deepening of convection at the leading edge (e.g., Mapes et al. 2006) is a primary goal for future development of this model.

The model is nonlinear, and many parameter choices affect the mean state as well as the existence or properties of time-dependent perturbations to it. Fig. 9 shows an example in which all parameters are the same as in Fig. 6, but the cloud-radiative feedback parameter r has been increased from 0.1 to 0.15. The mean state is dramatically changed, with strong rainfall everywhere and consequently much greater zonal mean rain rate than in Fig. 6. There are still self-sustained oscillations, but their properties are much different from those in Fig. 6. The wavelength is shorter, and the propagation is irregular; the disturbances

move predominantly westward, but with regular intervals of stationarity or slight eastward propagation.

The solution in fig. 9 illustrates the general property that changes in the perturbations are usually accompanied by changes in the mean state. It is not obvious whether the latter property is an advantage or disadvantage for an idealized MJO model. In full-physics general circulation models, changes in simulated MJO amplitude are also accompanied by mean state changes (Kim et al. 2011) (though not ones as large as here), and it is possible that interactions between the seasonal mean circulation and MJO disturbances are important in the real climate as well. If desired, various devices can be used to constrain the mean state in the present model, but these will in general also influence the disturbance dynamics.

We have performed a wide range of sensitivity studies. Solutions tend to resemble, qualitatively, one of those in figures 5-9, but a number of parameters influence which type of solution emerges. Besides δ and r — both of which are discussed above — the normalized gross moist stability $\tilde{M}$, the saturation column water vapor W_{max}, and the wind length scale L are also important. We do not present these studies here, as they are not yet particularly informative. The key result here is the emergence of the strongly nonlinear solution for positive δ in some parameter regimes. It is clear that this solution does not emerge for parameters which cause the background state to be very humid and rainy, as in figs. 8 or 9; such states tend to feature westward-propagating wavelike disturbances whose amplitude in precipitation is modest compared to the mean precipitation (though not necessarily small in absolute terms). The properties of the strongly nonlinear solution appear qualitatively similar in all cases in which it occurs, though there is some variation in the amplitude and spacing between disturbances.

c. Off-equatorial wind response function

The MJO tends to be strongest in southern hemisphere summer. Many MJO events have structures which are not symmetric about the equator, but rather have their greatest amplitude somewhat south of the equator (e.g., Wheeler and Kiladis 1999, fig. 7c). Off-equatorial MJO events have somewhat different wind structures than do equatorially symmetric ones, in a way that is qualitatively consistent with differences in the quasi-steady linear wind response to off-equatorial heating vs. equatorially symmetric heating. This off-equatorial behavior can be repesented in our model through differences in the wind response projection operator G.

Following our approach above for the equatorially symmetric case, we derive our off-equatorial G from the Gill (1980) solution to an off-equatorial heating. That is obtained by adding the solution for the equatorially symmetric heating (with meridional wave number $n = 1$) to the equatorially anti-symmetric heating with meridional wave number $n = 2$. We choose to evaluate the solution at a latitude $y = 1$ in units of equatorial deformation radii ($c/2\beta$, with c Kelvin wave speed and β planetary vorticity gradient). The resulting operator is

$$G(x|x') = -e^{-1/4} A e^{-[x-(x'+\delta)]/L}, \quad x > x' + \delta, \tag{29}$$

$$G(x|x') = 2e^{-1/4} A e^{3[(x-(x'+\delta)]/L} + 5A e^{5[(x-(x'+\delta)]/L}, \quad x < x' + \delta. \tag{30}$$

With this choice for G, the system becomes considerably more unstable, and exhibits a greater tendency towards the development of the nonlinear mode of behavior described in section 4 b. For the parameters used to generate figs. 5, 6, 7, and 8, (i.e., those shown in

table 1, apart from the changes in G) the nonlinear numerical code crashes after a short period of very rapid disturbance growth. Fig. 10 shows snapshots of precipitation and zonal wind (in the same format as figs. 6, 7, and 8,) from two nonlinear integrations using (29)-(30) with a couple of other parameter changes; these changes are chosen to reduce both the degree of instability in the model and the tendency to eastward propagation, to compensate for the change in G. The snapshots are taken at points where the disturbances are propagating at constant velocity with constant amplitude and shape. The left panel shows a calculation in which $\delta = 120$ km and $\tilde{M} = 0.2$. The doubling of $\tilde{M}$ relative to that shown in previous calculations stabilizes the model while the value of δ is positive, but small compared to that used to generate fig. 6. The right panel uses $\delta = 400$ km (the same as in fig. 6), $\tilde{M} = 0.15$ (intermediate between the value in the left panel and that used for preceding figures) while reducing the mean eastward wind from 5 to 1.7 $m\ s^{-1}$. The last change obviously reduces the tendency to eastward propagation relative to the planet surface, but also reduces the rate of disturbance growth for all but very small-amplitude disturbances.

Both calculations yield eastward-propagating nonlinear disturbances qualitatively similar to that in fig. 6. The amplitudes are quite different; note the different y-axis scales in the two panels. This is not deeply meaningful as the amplitude is quite sensitive to modest parameter changes, as discussed above. The propagation speeds are perhaps more interesting: approximately 12 $m\ s^{-1}$ for the left panel and 5.5 $m\ s^{-1}$ for the right, considerably larger than the basic state wind speeds of 5 and 1.7 $m\ s^{-1}$ respectively. This shows that this form for G, in which westerlies are strengthened relative to easterlies consistent with off-equatorial heating, increases the tendency to eastward propagation. Also, it shows that the propagation at almost precisely the speed of the basic state wind shown in fig. 6 is an

accident peculiar to the choice of G, rather than an inherent feature of the nonlinear mode. At least in some parameter regimes, the nonlinear mode is capable of producing eastward propagation *relative* to the basic state wind. Phase speeds comparable to those observed for the MJO in the warm pool region can be generated even for very weak basic state westerlies.

5. Conclusions

We have constructed a one-dimensional semi-empirical framework which we hope may be useful for developing MJO theories. The framework incorporates a number of strong assumptions, but is not based explicitly on a set of pre-defined vertical or meridional structures. This has the disadvantage that internal consistency is not enforced to the degree that it could be, but the advantage that the roles of key parameters or functions can be examined independently, and could in principle be determined based on observations or numerical modeling studies. While the particular implementation presented here can, under some circumstances, produce planetary-scale eastward-propagating disturbances, we do not claim at this point that these capture the essential dynamics of the MJO. We believe they capture hypotheses worth exploring, and use them as examples to demonstrate some sensitivities and basic properties of the framework.

In the linear regime, unstable normal modes exist but are all westward-propagating relative to the mean flow. Their growth rates and phase speeds are strongly sensitive to the convective time scale, which is a strong function of the mean state humidity. The spatial scale of the fastest growing mode is set by the scale of the quasi-stationary response of the wind to heating, which in reality depends on the effective stratification and damping that

act on the forced-dissipative waves that determine that response.

In some reasonable parameter regimes, if the projection function G which determines the zonal wind field as a function of precipitation is taken from the equatorially symmetric Gill model but is shifted a few hundred km to the east relative to precipitation, a nonlinear mode emerges which propagates eastward at the speed of the background eastward wind. The disturbances in this mode have a nearly sawtooth structure in humidity and precipitation maxima which decay exponentially westward and with a step function on the eastward side. If G is based on the equatorially asymmetric Gill solutions, the nonlinear mode emerges more readily, with less need for an eastward shift.

Extensions of the framework currently under exploration include: variations in the deterministic convective parameterization $P(W)$; addition of a stochastic component (either additive or multiplicative) to the convective parameterization; variable gross moist stability, parameterized as a function of column water vapor W or perhaps zonal wind u; zonal variation in the basic state; explicit (parameterized) representation of meridional advection, including eddy transports which may vary with MJO phase (Maloney 2009; Andersen and Kuang 2011); and coupling to a mixed layer ocean.

Acknowledgments

This work was supported by NASA grant NNX09AK34G (AHS), NOAA grants NA08OAR4320912 (AHS) and NA08OAR4320893 #7 and #14 (EDM), and NSF grants AGS-1008847 (AHS) and AGS-1025584 (EDM). We thank Daehyun Kim for a careful reading of the manuscript.

REFERENCES

Andersen, J. A. and Z. Kuang, 2011: Moist static energy budget of MJO-like disturbances in the atmosphere of a zonally symmetric aquaplanet. *J. Climate*, submitted.

Back, L. E. and C. S. Bretherton, 2006: Geographic variability in the export of moist static energy and vertical motion profiles in the tropical Pacific. *Geophys. Res. Lett.*, **33**, doi:10.1029/2006GL026 672.

Bantzer, C. H. and J. M. Wallace, 1996: Intraseasonal variability in tropical mean temperature and precipitation and their relation to the tropical 4050 day oscillation. *J. Atmos. Sci.*, **53**, 3032–3045.

Benedict, J. J. and D. A. Randall, 2007: Observed characteristics of the MJO relative to maximum rainfall. *J. Atmos. Sci.*, **64**, 2332–2354.

Benedict, J. J. and D. A. Randall, 2009: Structure of the Madden-Julian oscillation in the superparameterized CAM. *J. Atmos. Sci.*, **66**, 3277–3296.

Biello, J. A., A. J. Majda, and M. W. Moncrieff, 2007: Meridional momentum flux and superrotation in the multiscale IPESD MJO model. *J. Atmos. Sci.*, **64**, 1636–1651.

Bony, S. and K. A. Emanuel, 2005: On the role of moist processes in tropical intraseasonal variability: Cloud-radiation and moisture-convection feedbacks. *J. Atmos. Sci..*, **62**, 2770–2789.

Bretherton, C., M. E. Peters, and L. E. Back, 2004: Relationships between water vapor path and precipition over the tropical oceans. *J. Climate*, **17**, 1517–1528.

Bretherton, C. S., P. N. Blossey, and M. Khairoutdinov, 2005: An energy-balance analysis of deep convective self-aggregation above uniform sst. *J. Atmos. Sci.*, **62**, 4273–4292.

Bretherton, C. S. and A. H. Sobel, 2002: A simple model of a convectively coupled Walker Circulation using the weak temperature gradient approximation. *J. Climate*, **15**, 2907–2920.

Chen, S., R. A. Houze Jr., and B. E. Mapes, 1996: Multiscale variability of deep convection in relation to large-scale circulation in toga coare. *J. Atmos. Sci.*, **53**, 1380–1409.

Emanuel, K. A., 1987: An air-sea interaction model of intraseasonal oscillations in the tropics. *J. Atmos. Sci.*, **44**, 2324–2340.

Frierson, D. M. W., A. J. Majda, and O. Pauluis, 2004: Large scale dynamics of precipitation fronts in the tropical atmosphere: A novel relaxation limit. *Commun. Math. Sci.*, **2**, 591–626.

Fu, X., B. Wang, D. E. Waliser, and L. Tao, 2007: Impact of atmosphere-ocean coupling on the predictability of monsoon intraseasonal oscillations. *J. Atmos. Sci.*, **64**, 157–174.

Fuchs, Z. and D. J. Raymond, 2002: Large-scale modes of a nonrotating atmosphere with water vapor and cloud-radiation feedbacks. *J. Atmos. Sci.*, **59**, 1669–1679.

Fuchs, Z. and D. J. Raymond, 2005: Large-scale modes in a rotating atmosphere with radiative-convective instability and WISHE. *J. Atmos. Sci.*, **62**, 4084–4094.

Fuchs, Z. and D. J. Raymond, 2007: A simple, vertically resolved model of tropical disturbances with a humidity closure. *Tellus*, **59A**, 344–354.

Gill, A. E., 1980: Some simple solutions for heat induced tropical circulations. *Quart. J. Roy. Meteor. Soc.*, **106**, 447–462.

Gill, A. E. and P. J. Phlips, 1986: Nonlinear effects on heat-induced circulation of the tropical atmosphere. *Quart. J. Roy. Meteor. Soc.*, **112**, 69–91.

Grabowski, W. W., 2006: Impact of explicit atmosphere-ocean coupling on MJO-like coherent structures in idealized aquaplanet simulations. *J. Atmos. Sci.*, **63**, 2289–2306.

Haertel, P. T., G. N. Kiladis, A. Denno, and T. M. Rickenback, 2008: Vertical-mode decompositions of 2-day waves and the Madden-Julian oscillation. *J. Atmos. Sci.*, **65**, 813–833.

Hendon, H. H., 2000: Impact of air-sea coupling on the Madden-Julian oscillation in a general circulation model. *J. Atmos. Sci.*, **57 (24)**, 3939–3952.

Houze Jr., R. A., S. S. Chen, D. E. Kingsmill, Y. Serra, and S. E. Yuter, 2000: Convection over the pacific warm pool in relation to the atmospheric Kelvin-Rossby wave. *J. Atmos. Sci.*, **57**, 3058–3089.

Inness, P. M. and J. M. Slingo, 2003: Simulation of the Madden-Julian oscillation in a coupled general circulation model. Part I: Comparison with observations and an atmosphere-only GCM. *J. Climate*, **16**, 345–364.

Kemball-Cook, S., B. Wang, and X. Fu, 2002: Simulation of the intraseasonal oscillation in

the ECHAM-4 model: the impact of coupling with an ocean model. *J. Atmos. Sci.*, **59**, 1433–1453.

Kemball-Cook, S. R. and B. C. Weare, 2001: The onset of convection in the Madden-Julian Oscillation. *J. Climate*, **14**, 780–793.

Kiladis, G. N., K. H. Straub, and P. T. Haertel, 2005: Zonal and vertical structure of the Madden-Julian oscillation. *J. Atmos. Sci.*, **62**, 2790–2809.

Kiladis, G. N., M. C. Wheeler, P. T. Haertel, K. H. Straub, and P. E. Roundy, 2009: Convectively coupled equatorial waves. *Rev. Geophys.*, **47**, doi:10.1029/2008RG000 266.

Kim, D., A. H. Sobel, E. D. Maloney, D. M. W. Frierson, and I.-S. Kang, 2011: A systematic relationship between intraseasonal variability and mean state bias in AGCM simulations. *J. Climate, submitted.*

Kuang, Z., 2011: The wavelength dependence of the gross moist stability and the scale selection in the instability of column integrated moist static energy. *J. Atmos. Sci.*, **68**, 61–74.

Landu, K. and E. D. Maloney, 2011: Understanding intraseasonal variability in an aqua-planet gcm. *J. Meteor. Soc. Japan*, in press.

Lin, J. and B. E. Mapes, 2004: Radiation budget of the tropical intraseasonal oscillation. *J. Atmos. Sci.*, **61**, 2050–2062.

Lin, J., C. Zhang, and B. E. Mapes, 2004: Zonal momentum budget of the Madden-Julian

oscillation: The source and strength of equivalent linear damping. *J. Atmos. Sci.*, **62**, 21722188.

Madden, R. A. and P. R. Julian, 1971: Detection of a 40-50 day oscillation in the zonal wind in the tropical Pacific. *J. Atmos. Sci.*, **28**, 702–708.

Majda, A. J. and B. Khouider, 2001: A numerical strategy for efficient modeling of the equatorial wave guide. *Proc. Nat. Acad. Sci.*, **98**, 1341–1346.

Majda, A. J. and S. N. Stechmann, 2009: The skeleton of tropical intraseasonal oscillations. *Proc. Nat. Acad. Sci.*, **106**, "8417–8422".

Maloney, E. D., 2009: The moist static energy budget of a composite tropical intraseasonal oscillation in a climate model. *J. Climate*, **22**, 711–729.

Maloney, E. D. and J. Shaman, 2008: Intraseasonal variability of the west African monsoon and Atlantic ITCZ. *J. Climate*, **21**, 2898–2918.

Maloney, E. D. and A. H. Sobel, 2004: Surface fluxes and ocean coupling in the tropical intraseasonal oscillation. *J. Climate*, **17**, 4368–4386.

Maloney, E. D. and A. H. Sobel, 2007: Idealized hot spot experiments with a general circulation model. *J. Climate*, **20**, 908–925.

Maloney, E. D., A. H. Sobel, and W. M. Hannah, 2010: Intraseasonal variability in an aquaplanet general circulation model. *J. Adv. Model Earth Sys.*, **2**, DOI:10.3894/JAMES.2010.2.5.

Mapes, B., S. Tulich, J. Lin, and P. Zuidema, 2006: The mesoscale convection life cycle: Building block or prototype for large-scale tropical waves? *Dyn. Atmos. Oceans*, **42**, 3–29.

Miyakawa, T., Y. N. Takayabu, T. Nasuno, H. Miura, M. Satoh, and M. Moncrieff, 2011: Convective momentum transport by rainbands within a Madden-Julian oscillation in a global nonhydrostatic model with explicit deep convective processes. part i: Methodology and general results. *J. Atmos. Sci., submitted*.

Muller, C. J., L. E. Back, P. A. O'Gorman, and K. A. Emanuel, 2009: A model for the relationship between tropical precipitation and column water vapor. *Geophys. Res. Lett*, **36**, "L16 804, doi:10.1029/2009GL039 667".

Neelin, J. and J. Yu, 1994: Modes of tropical variability under convective adjustment and the Madden-Julian Oscillation. Part I: Analytical theory. *J. Atmos. Sci.*, **51**, 1876–1894.

Neelin, J. D., 1997: Implications of convective quasi-equilibrium for the large-scale flow. *The Physics and Parameterization of Moist Atmospheric Convection*, R. K. Smith, Ed., Kluwer, 413–446.

Neelin, J. D. and I. M. Held, 1987: Modeling tropical convergence based on the moist static energy budget. *Mon. Wea. Rev.*, **115**, 3–12.

Neelin, J. D., I. M. Held, and K. H. Cook, 1987: Evaporation-wind feedback and low-frequency variability in the tropical atmosphere. *J. Atmos. Sci.*, **44**, 2341–2348.

Neelin, J. D., O. Peters, and K. Hales, 2009: The transition to strong convection. *J. Atmos. Sci., in press*.

Pauluis, O., D. M. W. Frierson, and A. J. Majda, 2008: Precipitation fronts and the reflection and transmission of tropical disturbances. *Q. J. R. Meteor. Soc.*, **134**, 913–930.

Peters, O. and J. D. Neelin, 2006: Critical phenomena in atmospheric precipitation. *Nature Physics*, **2**, 393–396, doi:10.1038/nphys314.

Raymond, D. J., 2000: Thermodynamic control of tropical rainfall. *Quart. J. Roy. Meteor. Soc.*, **126**, 889–898.

Raymond, D. J., 2001: A new model of the Madden-Julian Oscillation. *J. Atmos. Sci.*, **58**, 2807–2819.

Raymond, D. J. and Z. Fuchs, 2009: Moisture modes and the Madden-Julian Oscillation. *J. Climate.*, **22**, 3031–3046.

Raymond, D. J., S. Sessions, A. H. Sobel, and Z. Fuchs, 2009: The mechanics of gross moist stability. *J. Adv. Model. Earth Sys.*, **1**, doi:10.3894/JAMES.2009.1.9.

Sarachik, E. S. and M. A. Cane, 2010: *The El Niño - Southern Oscillation Phenomenon.* Cambridge University Press.

Sessions, S., S. Sugaya, D. J. Raymond, and A. H. Sobel, 2010: Multiple equilibria in a cloud-resolving model. *submitted to J. Geophys. Res.*

Sherwood, S. C., 1999: Convective precursors and predictability in the tropical western Pacific. *Mon. Wea. Rev.*, **127**, 2977–2991.

Showman, A. P. and L. M. Polvani, 2010: The Matsuno-Gill model and equatorial superrotation. *Geophys. Res. Lett.*, **37**, L18 811, doi:10.1029/2010GL044 343.

Sobel, A. H., G. Bellon, and J. Bacmeister, 2007: Multiple equilibria in a single-column model of the tropical atmosphere. *Geophys. Res. Lett.*, **34**, L22 804,doi:10.1029/2007GL031 320.

Sobel, A. H. and C. S. Bretherton, 2003: Large-scale waves interacting with deep convection in idealized mesoscale model simulations. *Tellus*, **55**, 45–60.

Sobel, A. H. and H. Gildor, 2003: A simple time-dependent model of SST hot spots. *J. Climate*, **16**, 3978–3992.

Sobel, A. H., E. D. Maloney, G. Bellon, and D. M. Frierson, 2008: The role of surface fluxes in tropical intraseasonal oscillations. *Nature Geosci.*, **1**, doi:10.1038/ngo312.

Sobel, A. H., E. D. Maloney, G. Bellon, and D. M. Frierson, 2010: Surface fluxes and tropical intraseasonal variability: a reassessment. *J. Adv. Model. Earth Sys.*, **2**, doi:10.3894/JAMES.2010.2.2.

Sobel, A. H., J. Nilsson, and L. M. Polvani, 2001: The weak temperature gradient approximation and balanced tropical moisture waves. *J. Atmos. Sci.*, **58**, 3650–3665.

Sobel, A. H., S. E. Yuter, C. Bretherton, and G. N. Kiladis, 2004: Large-scale meteorology and deep convection during TRMM KWAJEX. *Mon. Wea. Rev.*, **132**, 422–444.

Stechmann, S. N. and A. J. Majda, 2006: The structure of precipitation fronts for nite relaxation time. *Theor. Comput. Fluid Dyn.*, **20**, 377–404.

Su, H. and J. D. Neelin, 2002: Teleconnection mechanisms for tropical Pacific descent anomalies during El Nino. *J. Atmos. Sci.*, **59**, 2694–2712.

Sugiyama, M., 2009a: Moisture mode in the tropics. Part I: Analysis based on the weak temperature gradient approximation. *Atmos. Sci.*, **66**, 1507–1523.

Sugiyama, M., 2009b: Moisture mode in the tropics. Part II: Nonlinear behavior on an equatorial β-plane. *J. Atmos. Sci.*, **66**, 1525–1542.

Tung, W.-W. and M. Yanai, 2002a: Convective momentum transport observed during the TOGA-COARE IOP. Part I: General features. *J. Meteor. Soc. Japan*, **59**, 1857–1871.

Tung, W.-W. and M. Yanai, 2002b: Convective momentum transport observed during the TOGA-COARE IOP. Part II: Case studies. *J. Meteor. Soc. Japan*, **59**, 2535–3549.

Waliser, D. E., K. M. Lau, and J. H. Kim, 1999: The influence of coupled sea surface temperatures on the Madden-Julian oscillation: A model perturbation experiment. *J. Atmos. Sci.*, **56 (3)**, 333–358.

Wheeler, M. and G. N. Kiladis, 1999: Convectively coupled equatorial waves: Analysis of clouds and temperature in the wavenumber-frequency domain. *J. Atmos. Sci.*, **56**, 374–399.

Zheng, Y., D. E. Waliser, W. F. Stern, and C. Jones, 2004: The role of coupled sea surface temperatures in the simulation of the tropical intraseasonal oscillation. *J. Climate*, **17**, 4109–4134.

Zhu, H., H. H. Hendon, and C. Jakob, 2009: Convection in a parameterized and super-parameterized model and its role in the representation of the MJO. *J. Atmos. Sci.*, **66**, 2796–2811.

Zurovac-Jevtic, D., S. Bony, and K. A. Emanuel, 2006: On the role of clouds and moisture in tropical waves: A two-dimensional model study. *J. Atmos. Sci.*, **63**, 2140–2155.

List of Figures

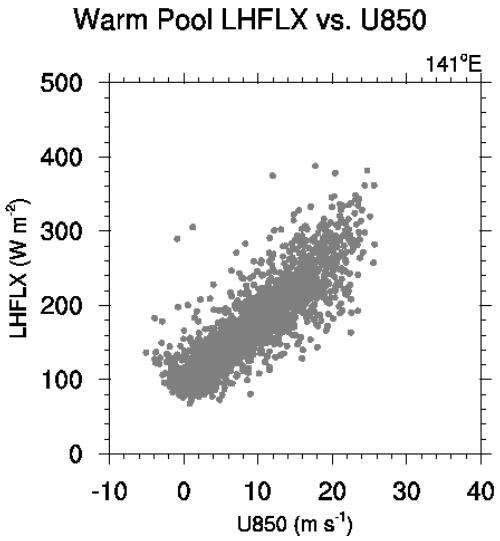

FIG. 1. Daily surface latent heat flux, on the y-axis, vs. 850 hPa zonal wind, on the x-axis, both quantities averaged from $0 - 20°$S at the longitude 141°E, from the aqua-planet simulation of Maloney et al. (2010).

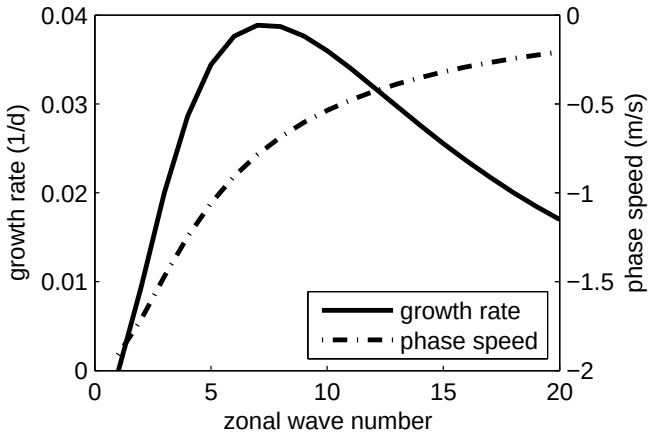

FIG. 2. Growth rate (solid, d^{-1}) and phase speed (dot-dash, $m\ s^{-1}$) For the linear model with a background value $W_0 = 45\ mm$ and a convective time scale $\tau_c = 2.4\ d$. Here the wind shift $\delta = 0$ and the background wind is assumed westerly, but the phase speed shown is that relative to the mean wind, rather than relative to the surface.

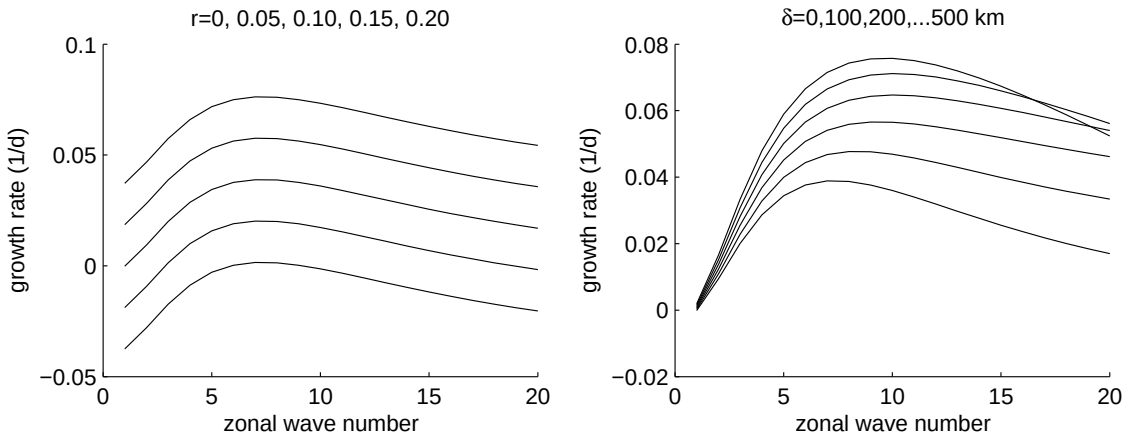

FIG. 3. Growth rate (d^{-1}) for the linear model with the same parameters as in fig. 2, except that on the left, the cloud-radiative feedback parameter r is varied from 0 to 0.2 in increments of 0.05, and on the right the wind shift parameter δ is varied from 0 to 500 km in increments of 100 km. Greater growth rate at low wave number corresponds to greater r and greater δ.

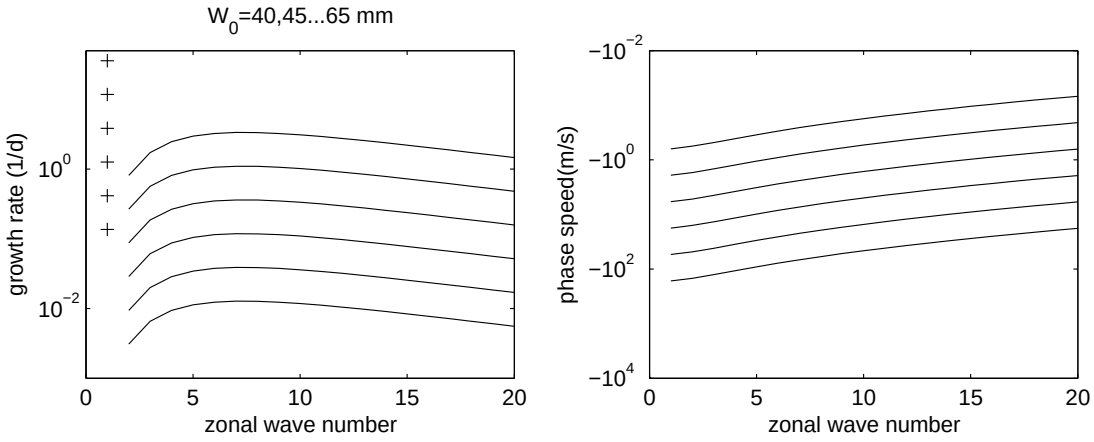

FIG. 4. Growth rate (left, d^{-1}) and phase speed (right, $m\ s^{-1}$) for the uncoupled linear model with the same parameters as in fig. 2, except that the background column water vapor W_0 is varied from 40 to 65 mm in increments of 5 mm; the saturation value is 70 mm. The inverse of the resulting linearized convective time scale, τ_c^{-1}, is shown by the red pluses on the left; τ_c itself varies from 7.3 to 0.03d. Smaller τ_c corresponds to larger growth rate and larger westward (more negative) phase speed.

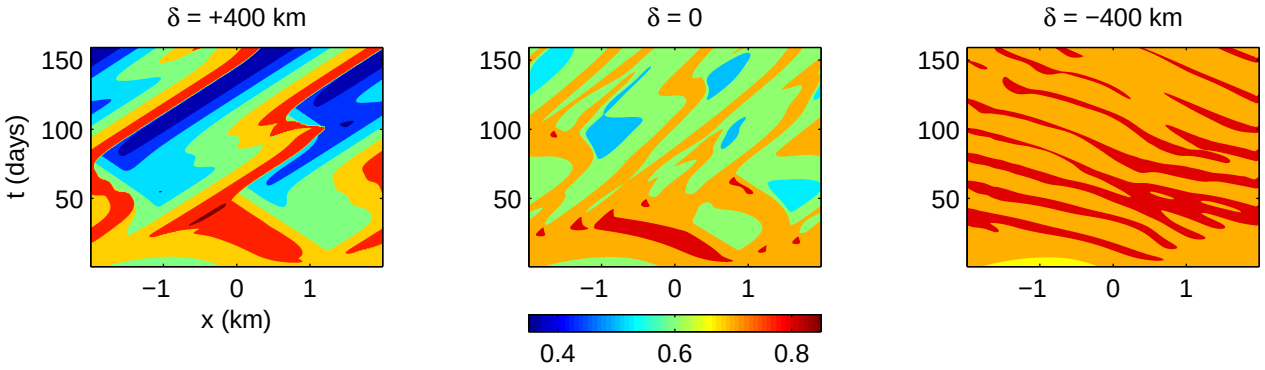

FIG. 5. Hovmoeller plots of saturation fraction W/W_{max} in integration with $\delta = 400,\ 0, -400$ km (left, middle, right), other parameters as in table 1. The x axes show longitudinal distance in units of 10,000 km while the y axes show time in days.

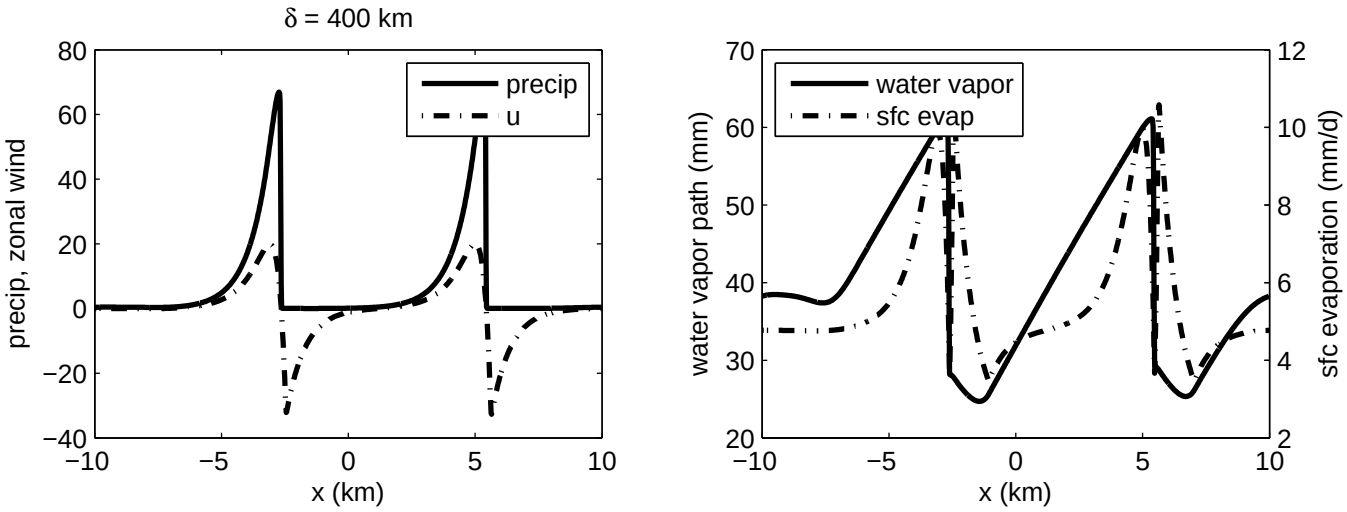

FIG. 6. Results from integration with $\delta = 400$ km, other parameters as in table 1. Both panels show snapshots at day 128 of perturbation zonal wind and precipitation (left, $m\ s^{-1}$ and $mm\ d^{-1}$, and water vapor path and surface latent heat flux (right, mm and and $mm\ d^{-1}$).

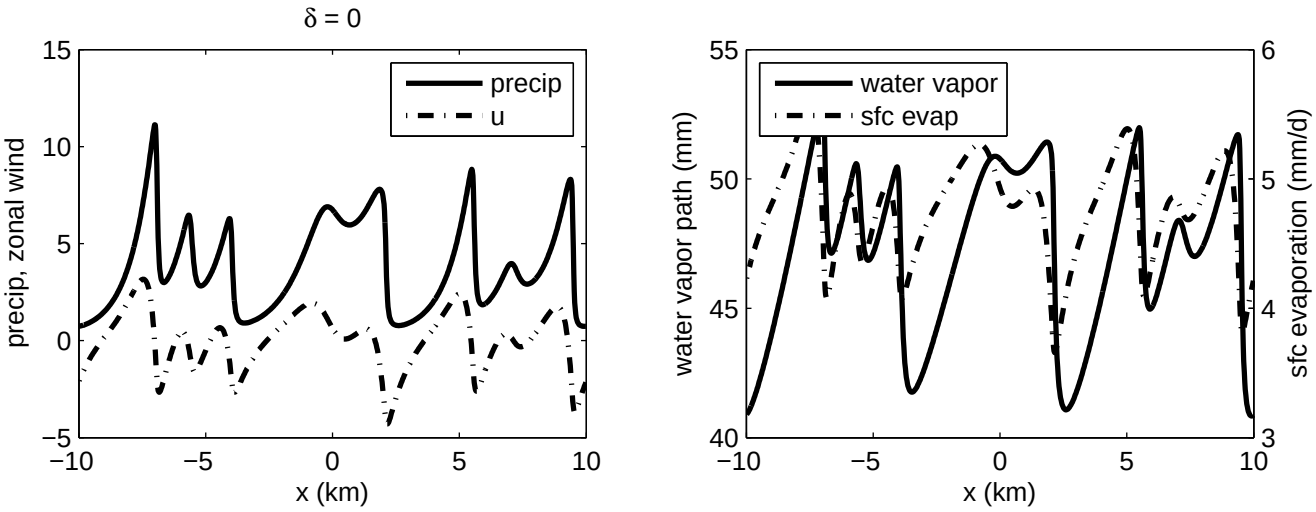

FIG. 7. As in fig. 6, but for $\delta = 0$.

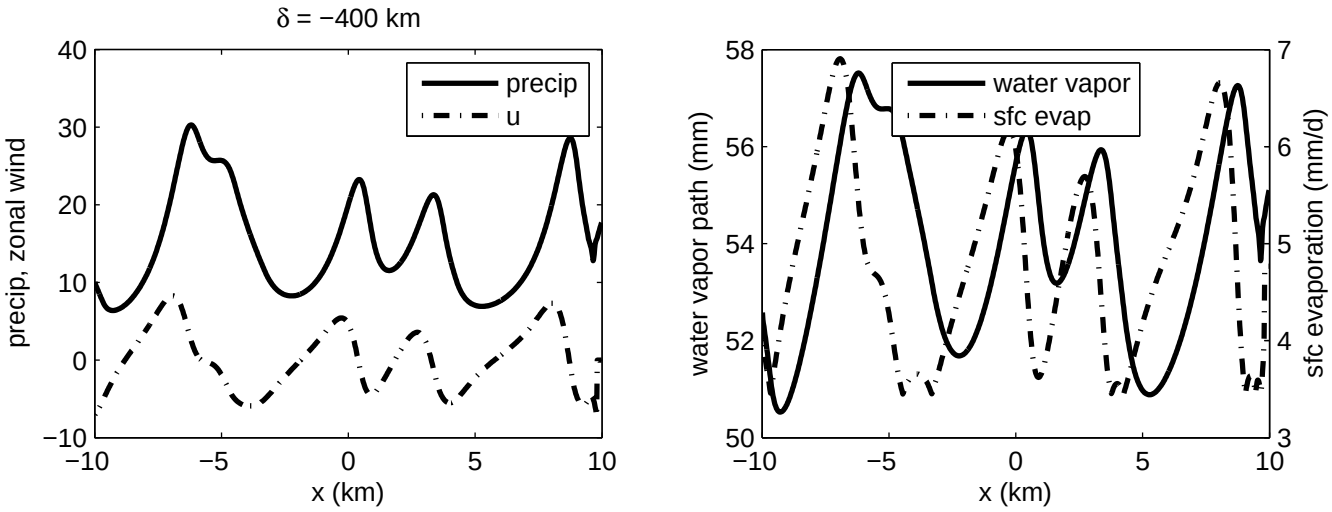

FIG. 8. As in fig. 6, but for $\delta = -400$ km.

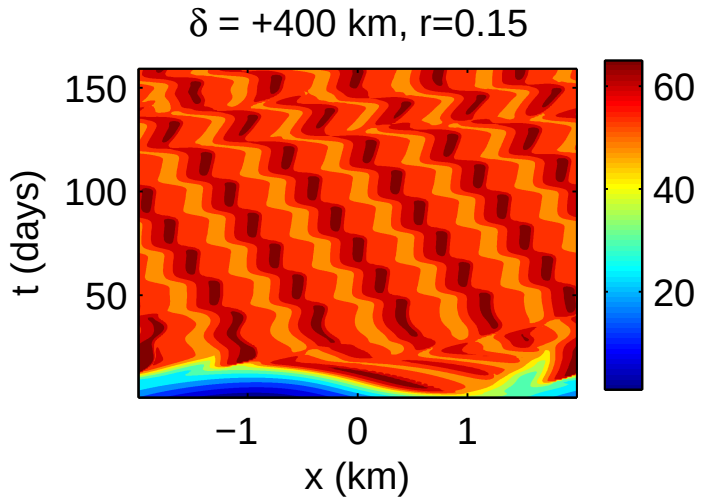

FIG. 9. As in fig. 5, but with $\delta = 400$ km and the radiative feedback parameter $r = 0.15$.

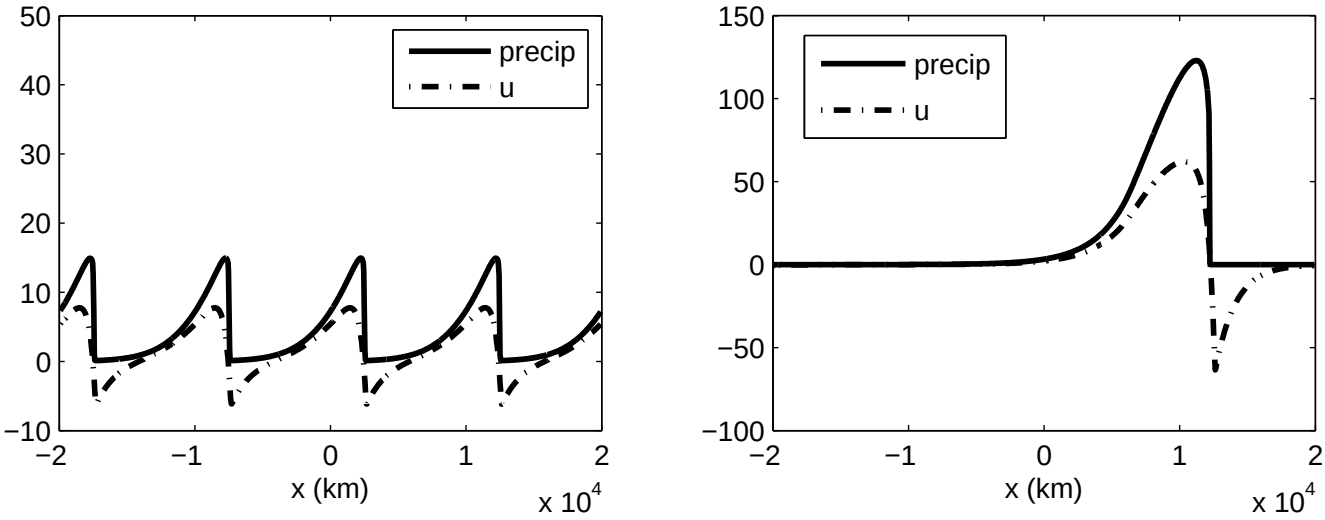

FIG. 10. As in figs. 6-8, but with the off-equatorial wind response function (29)-(30), and the additional following parameter changes. Left: $\delta = 120$ km and $\tilde{M} = 0.2$; right: $\delta = 400$ km (the same as in fig. 6), $\tilde{M} = 0.15$, and the background westerly wind is 1.7 $m\ s^{-1}$.

List of Tables

TABLE 1. Model parameter values.

parameter	value	Definition
R_0	4.8mm d^{-1}	Clear-sky radiative cooling
W_{max}	70 mm	Saturation column water vapor
$a_{dc},\ r_{dc}$	15.6, 0.603	constants in convective scheme
L	1500 km	length scale for wind response to precipitation
A	$0.8/L$ $(m\ s^{-1})(mm\ d^{-1})^{-1}m^{-1}$	Magnitude of wind response to precipitation
k	2604 $m^2\ s^{-1}$	diffusivity for moisture
U	5 m s^{-1}	background low-level zonal wind
$\tilde{M}$	0.1	Normalized gross moist stability (when fixed)
r	0.1	Cloud-radiative feedback parameter
$E_0,\ C_u$	100 W m^{-2}, 7.5 W m^{-2}	Sfc. LH flux for $u = 0$, LH flux change per $\|u\|$ in m s^{-1}